DJS Vol. 47(1) (2023) - pp. 63- 77 ISSN: 1012-5965

Delta Journal of Science

Available online at
https://djs.journals.ekb.eg/

Research Article **Physics**

Synthesis, Characterization, and Electrical Properties of La-Substituted Ni-Co-Sr Ferrites with Potential Applications

Nihal I. Mostafa[1], Aseel. M. Altarawneh[1], H.F. Abosheiasha[2], O. M. Hemeda[1], H. M. Ellabany[1], M. Z. Said[1], M. M. Salem[1*]

[1] Physics Department, Faculty of Science, Tanta University, 31527 Tanta, Egypt.
[2] Engineering Physics and Mathematics Department, Faculty of Engineering, Tanta University, Tanta, 31511, Egypt

[*]***Corresponding author:*** M. M. Salem ***E-mail:*** elshshtawy@science.tanta.edu.eg

Received: 10/9/2023 **Accepted:** 14/9/2023

KEY WORDS

Spinel ferrites, Lanthanum ion substitution, Nanomaterials, Thermal diffusivity, Thermal conductivity.

ABSTRACT

A set of $Ni_{0.45}Co_{0.45}Sr_{0.1}La_xFe_{2-x}O_4$ samples, with varying values of x (0, 0.02, 0.04, 0.06, 0.08, and 0.10), were synthesized using the flash auto-combustion method. The presence of the substituted La3+ ion in the system was verified via various characterization techniques, such as Scanning Electron Microscopy (SEM), Energy Dispersive X-ray (EDX) analysis, Dielectric Analysis, and Electrical Analysis. The morphology of all samples was examined utilizing field emission scanning electron microscopy (FE-SEM). The grain size measured from SEM increased by increasing lanthanum content up to the sample of lanthanum content x= 0.04, then decreased above this value. EDS spectra confirmed Co Ni Sr Fe for x=0.00 and indicate the presence of these elements beside lanthanum ion in the other samples, without the presence of contamination. At room temperature, the dielectric constant was studied for all samples ranging from 10^{-2} to 10^{8} Hz. At high frequency, the hopping rate increase and the ferrite material become more conductive, causing a rapid decrease of ε' and ε''. At lower frequencies, the inclusion of higher amounts of lanthanum leads to a reduction in the values of both ε' and ε''. The rise in Lanthanum content is associated with a drop in electric conductivity, which can be attributed to the rule governing the increase in grain resistance, resulting in a decrease in AC conductivity. Thermal conductivity and thermal diffusivity increase with temperature. Due to its characteristics, this material may be ideal for thermoelectric and thermomagnetic sensors and switches.

Introduction

The study and use of materials having dimensions between one and one hundred nanometers are the subjects of nanoscience and nanotechnology. The disciplines of physics, chemistry, chemical, electrical, and mechanical engineering are all involved in interdisciplinary research and technology at the nanoscale **(Anwar et al., 2020; Gilani et al., 2020; Kumar et al., 2012).**

Due to their applicability in many spheres of life, nanomaterials have attracted a great deal of attention during the past thirty years. Nanomaterials have a high surface-to-volume ratio, which causes changes in their physical and chemical characteristics to result in a wide range of uses and applications **(Kalia et al., 2023; Ramadevi et al., 2020; Koutsoumbou et al., 2021; Munir et al., 2022).** These applications encompass material qualities that are fundamentally distinct from bulk material, including mechanical, chemical, electrical, magnetic, and optical **(Gilani et al., 2020).**

Sol-gel, hydrothermal, combustion, mechano-chemical, precursor, microemulsion, and microwave refluxing techniques have all been employed to create nanocrystalline soft ferrites **(Yi et al., 2021).**

Various features of ferrite materials containing metal and iron oxide are utilized in technical and scientific applications. Ferrites exhibit a wide range of properties, including magnetic, electrical, optoelectronic, electrochemical, and magnetoelectronic ones. These ferrite characteristics are significantly influenced by the distribution of cations among the available interstitial sites, the nature and type of dopants, the synthesis parameters, and the synthesis techniques **(Gilani et al., 2020).**

Due to its superior and distinctive properties when compared to bulk spinel ferrites, nano-particle spinel ferrites have attracted the attention of many researchers. The tiny diameters of the nanoparticles helped in the development of theoretical and practical applications **(Chintala et al., 2021; Ahmad et al., 2022; Al-Bassami et al. 2023; Vinod et al., 2022).** A prominent kind of magnetic material known as spinel ferrite combines the two-dimensional characteristics of an electrical insulator and a magnetic conductor. A spinel structure that is formed by a nearly close-packed FCC array of anions with holes partly filled by the cations can be represented by the formula AB_2O_4 **(Slatineanu et al., 2013; Hossain et al., 2022; Manohar et al., 2021).** The

oxygen atoms are placed in a cubic pattern, with A and B referring to the tetrahedral and octahedral sites in the crystal structure of spinel ferrites, and the oxygen atoms are arranged in a cubic arrangement, with A and B denoting the tetrahedral and octahedral sites, respectively **(Hamza et al., 2022; Iranmanesh et al., 2018).** Spinel ferrites' high saturation magnetization, high permeability, and exceptionally high electrical resistivity are some of its finest qualities at high frequencies. The inverse spinel ferrites, cobalt ferrites, nickel ferrites, and strontium ferrites are some of the spinel ferrites **(Kokare et al., 2018).**

Due to their distinctive characteristics, cobalt ferrite is significantly more essential than other spinel ferrite **(Almessiere et al., 2021).** Elevated Curie temperature, strong Coercivity, outstanding magneto-crystalline alignment, decent saturation magnetization, robust mechanical resilience, and chemical durability. **(Pubby et al., 2020).** These features make cobalt ferrite a strong option for a variety of applications. Cobalt ferrites play an important role in the development of microwave and spintronic devices, solar cells, magnetostrictive sensors, drug delivery systems, transducers, actuators, lithium-ion batteries, supercapacitors, and computer memory components **(Ramadevi et al., 2020; Koutsoumbou et al., 2021).** Nickel ferrites have the same properties as Co ferrites **(Kokare et al., 2018).**

As a member of the spinel ferrite family with high electrical resistivity, high saturation magnetization, high Curie temperature, low eddy current, and low dielectric losses, nickel ferrite is one of the best options for usage in these applications **(Hussain et al., 2023; Chintala et al., 2021).** Ni ferrites are therefore utilized as a magnetic material in the disciplines of power application, antenna manufacturing, computer memory, catalysts, energy storage in supercapacitors, biotechnology, and high-density information storage., electrical and electronic devices **(Narang et al., 2021).** Ni ferrite has a larger magneto-crystalline anisotropy constant than its bulk, the corresponding one, which makes it a candidate for high-frequency application **(Rana et al., 2021).**

Strontium ferrite is one type of ceramic ferrite magnet. The strontium ferrite is a hard ferrite that has many applications in memory storage and magnetic recording media **(Zhang et al., 2021; Óvári et al., 2017; Ateia et al., 2017).**

The current investigation aims to analyze the influence of La^{3+} ions on the structural characteristics of Ni-Co-Sr spinel and interested in the impact of rare earth element on thermo-magnetic properties of ferrite and directing it for application of heat transfer application.

Experimental details:

In the present study, Ni-Co-Sr-La spinel ferrites characterized by the chemical formula $Ni_{0.45}$ $Co_{0.45}$ $Sr_{0.1}$ La_x $Fe_{2-x}O_4$ where (x= 0.00, 0.02, 0.04, 0.06, 0.08, and 0.10) were prepared by the flash auto combustion method as illustrated in **Fig. (1)**. The morphology of ferrite samples was characterized utilizing a Scanning Electron Microscope (SEM) with the specific model being JOEL, Model: JSM-5200 LV. The Broadband Dielectric Spectrometer (BDS) employs the NoVo control concept, namely the 40 Broadband dielectric spectrometer model and Alpha impedance analyzer, to accurately assess the dielectric and electrical properties within a frequency range of 10^{-2} to 10^{8} Hz. The samples' dielectric constant (ε), dielectric loss, and electrical resistivity were studied at different temperatures using an RLC bridge known as the BM591. The thermal constants analyzer, known as the hot disk, employs a sensor consisting of concentric rings arranged in a double spiral configuration. This sensor serves a dual purpose: it functions as a planar heater to raise the temperature of the sample. Also, it operates as an Ohmic resistance thermometer to measure the time-dependent temperature rise. The spiral, composed of nickel material and coated with Kapton on both sides to safeguard and provide electrical insulation, is conveniently positioned amidst two sample sections under examination. During the experimental procedure, a minute and unchanging electrical current is administered, wherein the resultant voltage produced by the sensor exhibits a direct relationship with the prevailing temperature. The throttle position (TPS) sensor with a radius of 2.1 mm was inserted between two uniform disks of the same sample, each having a diameter of 15 mm and a thickness of approximately 3 mm. The output power was held constant at 20 milliwatts (mW). At the same time, the total duration of the measurements ranged from 10 seconds (s) to 20 seconds (s). Notably, the observed temperature variation on the sample's surface is directly associated with the measured thermal conductivity. The output power remained consistent throughout all the measurements.

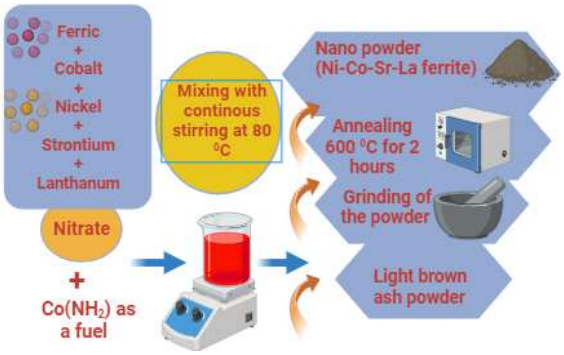

Fig. (1): Preparation of ferrites samples $Ni_{0.45}Co_{0.45}Sr_{0.1}La_xFe_{2-x}O_4$ using flash auto combustion technique.

Results and discussion

FE-SEM analysis

The morphology analysis of $Ni_{0.45}$ $Co_{0.45}$ $Sr_{0.1}$ Fe_2O_4 doped with lanthanum content where (X= 0.00, 0.02, 0.04, 0.06, 0.08, and 0.10) were studied by field emission scanning electron microscope.

Figure (2) shows the surface morphology of the given structure and indicates the presence of irregular grain shapes for samples x= 0.00 and 0.02 and spherical grains for the other samples. It clearly showed some agglomeration for the grain structure **(Kokare et al., 2018).** The grain size obtained from SEM increased by increasing lanthanum content up to the sample of lanthanum content x=0.04, then decreased above this value **(Hasan et al., 2019).**

The grain size values of the given composition were around 66 nm for x= 0.00 and 130nm for x= 0.04, indicating the presence of the nanocrystalline nature of the samples **(Kokare et al., 2018), (Slatineanu et al., 2013).** For lanthanum content ≤ 0.04, the lanthanum ions enter the B-site and become soluble

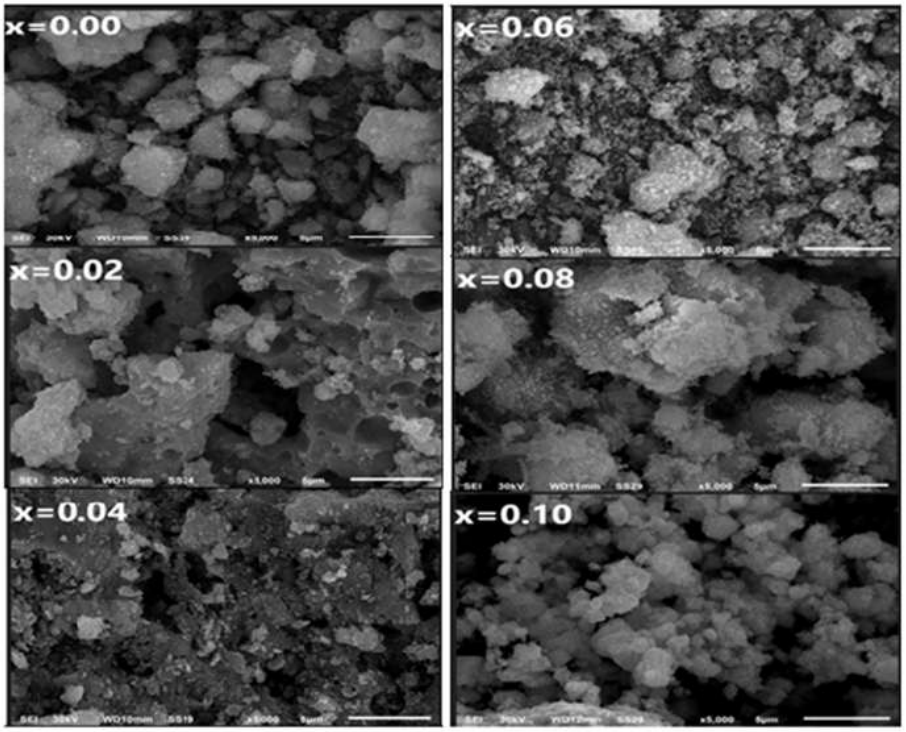

Fig. (2): SEM images for different La content.

in the lattice, which is the reason for the increase of the grain size up to this limit at x>0.04 the lanthanum ions become not soluble in the lattice and accumulate at the grain boundary leading to the decrease of the grain size and inhibit its growth **(Kokare et al., 2018).**

Figure (3) shows the EDX spectra, which confirm Co Ni Sr Fe for (x=0.00) and indicate the presence of these elements beside lanthanum ion for the other samples, without any contamination.

Table (1): Elements (Atomic%) of $Ni_{0.45}Co_{0.45}Sr_{0.1}La_xFe_{2-x}O_4$

x	Elements (Atomic %)					
	O k	Fe k	Cok	Ni k	Sr k	La l
0.00	63.40	24.73	6.08	5.21	0.57	0
0.02	50.86	31.12	9.19	6.16	2.17	0.49
0.04	64.12	24.53	5.25	4.62	0.98	0.50
0.06	65.45	22.83	5.02	4.73	1.27	0.7
0.08	63.51	24.47	5.39	4.68	0.83	1.12
0.10	65.5	22.06	5.47	4.69	0.73	1.56

Electrical and Dielectric Properties

Conductivity

Figure 4 shows the variation of the real and imaginary parts of AC conductivity as a function of the frequency of the studied samples with different lanthanum content. From the figure, it was noticed that the conductivity spectrum consists of two main regions, the first at low frequency, which is characterized by Plato, and the second at high frequency, which is characterized by dispersion region **(Hassan et al., 2023).** The Plato behavior at low frequency from 0.1 HZ to 10^5 HZ reflects the DC conductivity component of the samples at the second region from 10^5 HZ to 10^7 HZ. The spectrum follows John Schor's universal power law **(Ahmad, 2022).** In this region, the hopping ions and electrons to vacant positions quickly return to their original positions. Hence, the conductivity increases sharply with increasing frequency.

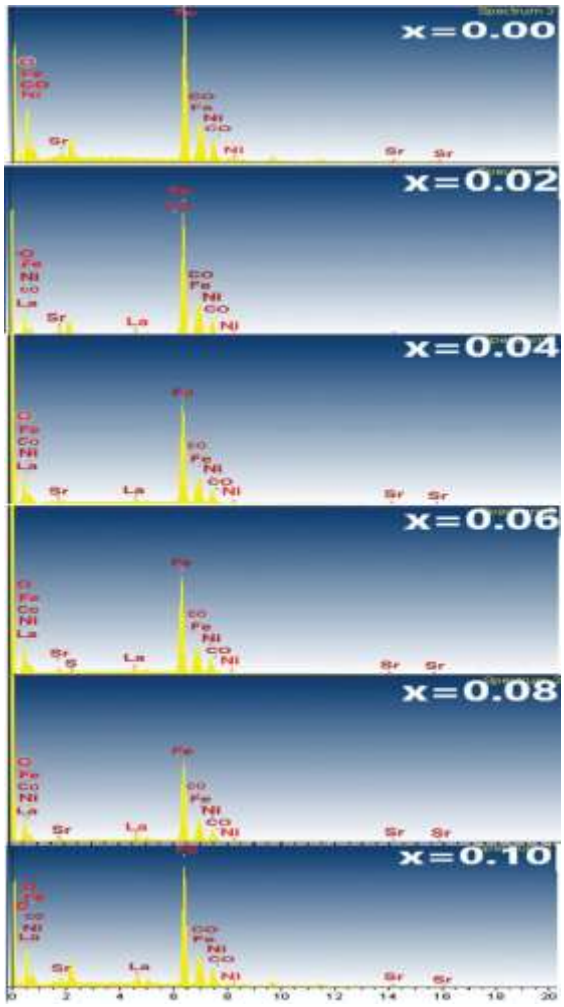

Fig. (3): EDX analysis of the resulting $Ni_{0.45}Co_{0.45}Sr_{0.1}La_xFe_{2-x}O_4$.

The power law is $\sigma_{AC} = \sigma_{DC} + A\omega^n$, where σ_{DC} is the DC-conductivity in continuous currents, and (A) and (n) are a constant and an exponent which reflects the degree of interaction between ions and their environment, respectively. , if n<1, the backward rate for hopping is slow, and if n**>**1, the backward hopping is faster than the relaxation time of the hopping position **(Sarmah et al., 2023).**

The frequency at which the conductivity changes its behavior is called the hopping frequency **(Amorri et al., 2023).** The figure also shows the electric conductivity increase by increasing Lanthanum content, which is related to the rule of grain resistance decrease leading to the increase of AC conductivity. The behavior of **σ"** vs. frequency reflects the reverse behavior of ***σ′*** **(Amorri et al., 2023).**

The dielectric permittivity frequency

The behavior of the dielectric permittivity ε′ and ε" as a function of frequency from 1 Hz to 10^7 Hz are shown in **Fig. (5)**. It was noticed from the figures that ε′ and ε"have high values around 0.1 Hz. Above this frequency, the ε′ and ε" are almost frequency-independent at high frequencies up to 10^7 Hz **(Hussain et al., 2023).** We can discuss the dependency of dielectric permittivity vs. frequency using Koop's and Maxwell-Wagner models, where they consider the dielectric properties of ferrites depend on the grain boundaries, which are good conductors and the inter-grains with the presence of pores are poor conductors. The materials that belong to Koop's model can be described as parallel combinations of two capacitances and two resistances **(Routray et al., 2020).**

Generally, the έ of ferrite describes the stored energy in the material, where ε " shows the energy loss and shifted by 90° in phase with ε′. The grain boundary is more active at low frequencies, which induces interfacial and space charge polarization. At the same time, the electron hopping process decreases at high frequency, leading to the decrease of ε′. By increasing frequency, the hopping rate increase and the ferrite material become more conductive, causing a rapid decrease of ε' and ε''. The increase of lanthanum content at low frequency decreases the values of ε′ and ε". The presence of lanthanum ions at the octahedral site decreases the bond length of Fe^{3+}- O^{2-} leading to the increase of hopping rate, consequently decrease of ε′and ε".

Figure (5) represents the tangent loss (tan(δ)) of the studied samples with different lanthanum content as a function of frequency from 0.1 Hz to 10^7 Hz at

room temperature. The tanδ can be calculated from the formula $\tan\delta = \frac{\varepsilon''}{\varepsilon'}$ **(Hussain et al., 2023).** In our case, we didn't calculate tanδ but measured it from the device given in the experimental section. Tanδ has high values at low frequencies and reaches maximum at certain frequencies due to the relaxation process, which is associated with the relaxation time and is given in **Table (2)**. The given values of tanδ at low frequency may be because the hopping electrons frequency can follow the variation of the AC applied field. However, tan(δ) has small values when the electron hopping doesn't follow the applied electric field frequency **(Akhtar et al., 2023).** We can see from the figure that the tanδ is high at low frequency, and it exponentially decreases as frequency increases.

At low frequencies, the grain boundaries are more active, reflecting high values of tan(δ) **(Deonikar et al., 2020).** By increasing frequency, the hopping electron process becomes easy, and hence, the hopping rate increases, the material becomes more conductor, which causes the rapid decrease in tanδ and the hopping rate frequency will not respond to the external AC applied frequency **(P. Kumar et al., 2010).** The loss factor tanδ has maximum values at low frequencies.

The **Fig. (5)** depicts the loss tangent variations with different lanthanum contents. The value of tanδ increases at sample x= 0.02 La content and then decreases for the other samples, and the sample x=0.10 has a low value of tan(δ). The value x= 0.02 has the highest conductivity value and the tan(δ) value. By increasing lanthanum contents, the values of conductivity decrease and consequently, the tan(δ) values decrease

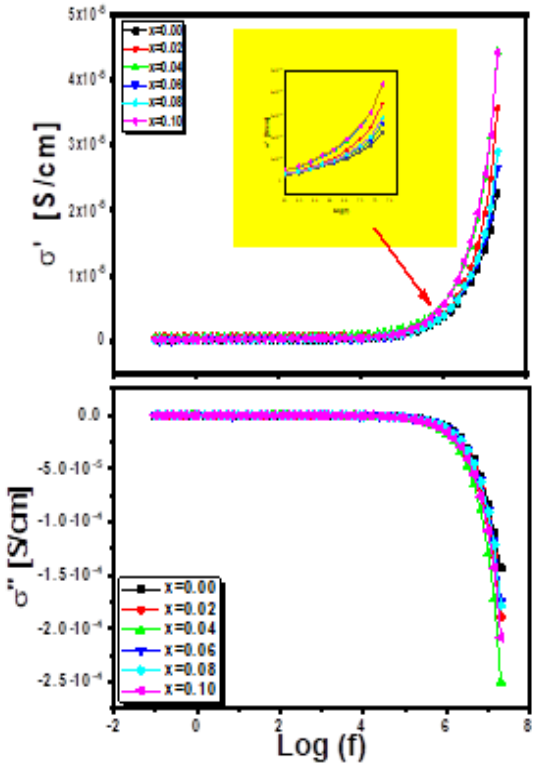

Fig. (4): The real part and imaginary part of conductivity

Table (2): Relaxation time of tangent loss and M", grain size

x	$\tau_{Tan(\delta)}$(sec)	$\tau_{M''}$(sec)	Grain size(nm)
0.00	$3.539x10^{3}$	$0.03x10^{-5}$	0.066
0.02	$7.441x10^{3}$	$0.16x10^{-5}$	0.070
0.04	$2.441x10^{3}$	$0.10x10^{-5}$	0.130
0.06	$2.441x10^{3}$	$0.02x10^{-5}$	0.083
0.08	$2.441x10^{3}$	$0.03x10^{-5}$	0.081
0.10	$1.592x10^{3}$	$0.05x10^{-6}$	0.071

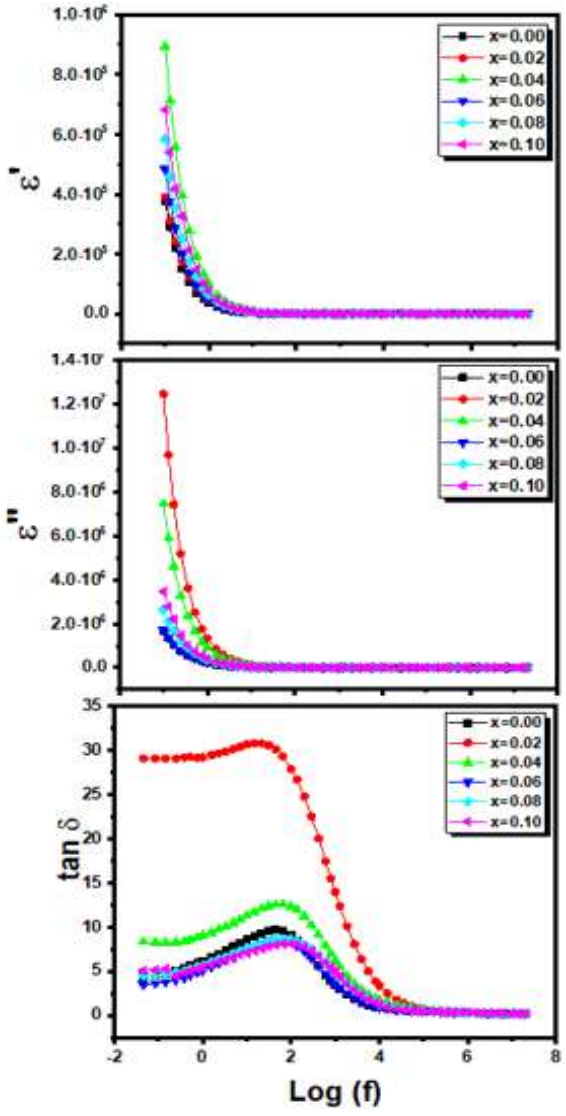

Fig. (5): the real part and the imaginary part of the dielectric constant, and the loss tangent

Thermal properties (thermal conductivity and thermal diffusivity):

The thermal conductivity and thermal diffusivity of $Ni_{0.45}Co_{0.45}Sr_{0.1}La_xFe_{2-x}O_4$ where (X=0.00,0.02,0.04,0.06,0.08 and 0.10) samples were measured at different temperature from room temperature to 260℃ using the hot disk thermal constants analyzer. The thermal conductivity of the samples increases by increasing temperature and has the highest value for the sample x=0.04 of lanthanum content; as shown in **Fig.(6),** the thermal conductivity and thermal diffusivity were enhanced by the doping of lanthanum with x= 0.02 and 0.04, then decrease again for other samples. The increase of thermal conductivity and diffusivity were increased by doping of lanthanum ions may be due to the formation of conducting chains in the crystal lattice where heat can follow easily. The highest thermal conductivity and diffusivity were achieved for x=0.02 and x= 0.04 of lanthanum content, where these samples' electrical conductivity, grain size, and saturation magnetization are also high values. These results may lead us to a strong correlation between our ferrite samples' grain size, electrical conductivity, and thermal behavior. Similar results were given in previous work for (M–$CoFe_2O_4$ (where M=Cu and Zn)) **(El-masry et al., 2023).** The

values of thermal conductivity and diffusivity in the temperature range from room temperature to 260 ℃ are given in **Table (3)**. The value of thermal conductivity and thermal diffusivity are in agreement with the previous work (El-**masry et al., 2023).** The thermal conductivity of ferrites generally has a low value and ranges from 5.8 to 7.9 W/mK **(Chen and Tuan, 2021).**

Table (3): Thermal conductivity and diffusivity of the published data and our present data for different La content

X	Thermal conductivity (W/mK)	Thermal diffusivity (mm^2/s)	Reference
0.00	0.4359-0.4563	0.1881-0.2145	present work
0.02	0.3562-0.4610	0.4429-0.3528	present work
0.04	0.4523-0.5156	0.4630-0.4068	present work
0.06	0.3466-0.3892	0.1657-0.2089	present work
0.08	0.3735-0.4402	0.1911-0.2004	present work
0.10	0.1530-0.4004	0.1530-0.1727	present work
$CoFe_2O_4$	0.6	0.52	(El-masry et al., 2023)
$CuCoFe_2O_4$	0.95	0.75	
$ZnCoFe_2O_4$	0.82	0.6	

The observed increase in thermal conductivity and thermal diffusivity with temperature is due to the presence of the normal scattering process. The factors that affect the variation of thermal conductivity and thermal diffusivity are the phonon scattering mechanism, like stray scattering, defects, and structural scattering **(Tariq et al., 2015).**

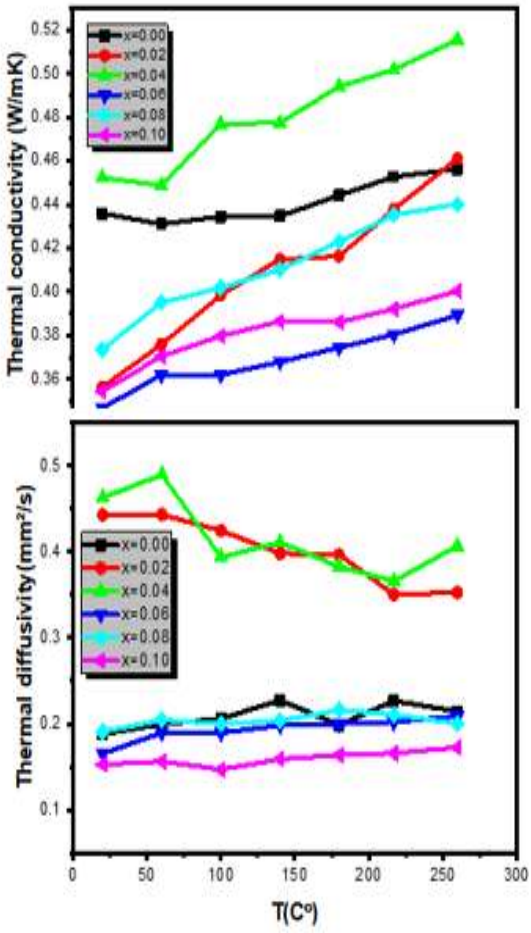

Fig. (6): Thermal conductivity and Therma diffusivity vs. T of $Ni_{0.45}Co_{0.45}Sr_{0.1}La_xFe_{2-x}O_4$.

Conclusions

Nano-sized $Ni_{0.45}Co_{0.45}Sr_{0.1}La_xFe_{2-x}O_4$ ferrites with varying La content (x =0.00, 0.02, 0.04, 0.06, 0.08, 0.10) were synthesized using the flash auto-combustion technique. This study investigates how the substitution of La^{3+} for Fe^{3+} affects the structure, morphology, and magnetic properties of Ni-Co-Sr ferrite nanocrystals. The incorporation of lanthanum ions had a noticeable impact on the properties of

Ni-Co-Sr ferrite, particularly in terms of electron movement and variations in dielectric constant (ε′) and loss tangent (tanδ) with respect to frequency and composition. The introduction of La^{3+} ions into the Ni-Co-Sr ferrite material resulted in ferrites with high ε′ and low tanδ, making them suitable for high-frequency applications. Thermal conductivity and thermal diffusivity were found to increase with La doping at x = 0.02 and 0.04 concentrations but decreased for subsequent samples. Ni-Co-Sr ferrite exhibits diverse applications, including heat transfer in automotive systems, magnetic sealing, heat exchangers, liquid-cooled computers, fuel cells, heat pipes, and heat pumps.

Reference

Ahmad, Syed Ismail. 2022. "Nano Cobalt Ferrites: Doping, Structural, Low-Temperature, and Room Temperature Magnetic and Dielectric Properties – A Comprehensive Review." *J. Mag. Mag. M.* 562 (August): 169840.

https://doi.org/10.1016/j.jmmm.2022.169840.

Akhtar, S., M. A. Almessiere, B. Unal, A. Demir Korkmaz, Y. Slimani, N. Tashkandi, A. Baykal, A. Ul-Hamid, and A. Manikandan. 2023. "Electrical and Dielectric Properties of $Ni_{0.5}Co_{0.5}Ga_xFe_{1.8-X}O_4$ ($x \leq 1.0$) Spinel Ferrite Microspheres." *J. R. E.* 41 (2): 259–67.

https://doi.org/10.1016/j.jre.2022.01.021.

Al-Bassami, N. S., S. F. Mansour, E. Abdel-Fattah, and M. A. Abdo. 2023. "Ce-Co-Mn-Zn Ferrite Nano Catalyst: A Synergetic Effect of Rare Earth Ce^{3+} on Enhanced Optical Properties and Photocatalysis." J. *C. Int*. 49(12): 20601–12.

https://doi.org/10.1016/j.ceramint.2023.03.191.

Almessiere, M A, S Güner, M Sertkol, A Demir Korkmaz, A Baykal, I A Auwal, S E Shirsath, Y Slimani, and M Hassan. 2021. "Comparative Study of Sonochemically and Hydrothermally Synthesized $Mn_{0.5}Zn_{0.5}Sm_xEu_xFe_{2-2x}O_4$ Nanoparticles: Structural, Optical and Magnetic Properties." *J. N. S & N. Obj* 28: 100792.

https://doi.org/https://doi.org/10.1016/j.nanoso.2021.100792.

Amorri, O., M. Khalfa, A. Oueslati, K. Khirouni, A. Aydi, and E. Dhahri. 2023. "Effects of the Substitution by Copper on Structural, Optical and Dielectric Properties of the Spinel $LiFe_2O_4$." *J. M. Ch. Phy*. 127753.

https://doi.org/10.1016/j.matchemphys.2023.127753.

Anwar, Asima, Sonia Zulfiqar, Muhammad Asif Yousuf, Sameh A. Ragab, Muhammad Azhar Khan, Imran Shakir, and Muhammad Farooq Warsi. 2020. "Impact of Rare Earth Dy^{+3} Cations on the Various Parameters of Nanocrystalline Nickel Spinel Ferrite." *J. M. R. and Tech*. 9(3): 5313–25.

https://doi.org/10.1016/j.jmrt.2020.03.057.

Ateia, Ebtesam E., E. Takla, and Amira T. Mohamed. 2017. "Physical and Magnetic Properties of (Ba/Sr) Substituted Magnesium Nano Ferrites." J. *App. Phy.* A 123(10).

https://doi.org/10.1007/s00339-017-1246-1.

Chen, Guan-ren, and Wei-hsing Tuan. 2021. "Bonding Microwave Absorbing Ferrites to Thermal Conducting Copper," no. August: 1001–8.

https://doi.org/10.1111/ijac.13859.

Chintala, J. N.Pavan Kumar, S. D. Kaushik, M. Chaitanya Varma, G. S.V.R.K. Choudary, and K. H. Rao. 2021. "An Accurate Low Temperature Cation Distribution of Nano Ni-Zn Ferrite Having a Very High Saturation Magnetization." *J. Sup. and Nov. Mag.* 34(1):149–56.

https://doi.org/10.1007/s10948-020-057283.

Deonikar, Virendrakumar G, Vasudev D Kulkarni, Sopan M Rathod, and Hern Kim. 2020. "Fabrication and Characterizations of Structurally Engineered Lanthanum Substituted Nickel-Cobalt Ferrites for the Analysis of Electric and Dielectric Properties." J. In. Ch. Comm., 119: 108074.

https://doi.org/https://doi.org/10.1016/j.inoche.2020.108074.

El-masry, Mai M, Abd El-razek Mahmoud, H Y Morshidy, and Rania Ramadan. 2023. "Cu^{2+}-and Zn^{2+} -Doped Cobalt Spinel Ferrite : Insights on Structural, Thermal Conduction, Electric, Magnetic and Elastic Properties." *J. M. Sci.*

https://doi.org/10.1007/s10854-022-09777-3.

Gilani, Zaheer Abbas, Amir Farooq, Noor ul Huda Khan Asghar, and Muhammad Khalid. 2020. "Synthesis and Characterization of Lanthanum Doped Co-Zn Spinel Ferrites Nanoparticles by Sol-Gel Auto Combustion Method." *J. M. Phys. Sci.* 1 (1): 1–11.

https://doi.org/10.52131/jmps.2020.0101.0001.

Hamza, Muhammad, Atiq ur Rehman, Ihsan Ali, Muhammad Asif, and Mukhtar Ahmad. 2022. "Detailed Analysis of Lanthanum Impact on Structural, Morphological and Magnetic Properties of Manganese Spinel Ferrites ($MnLa_xFe_{2-X}O_4$ X = (0.0, 0.1, 0.2) Synthesized through Hydrothermal Technique." *J. Mag. Mag. M.* 564 (August).

https://doi.org/10.1016/j.jmmm.2022.169852.

Hasan, M. S., M. I. Arshad, A. Ali, K. Mahmood, N. Amin, S. S. Ali, M. I. Khan, G. Mustafa, M. J. Khan, and M. Saleem. 2019. "Mg and La Co-Doped ZnNi Spinel Ferrites for Low Resistive Applications." *J. M. Res. Exp.* 6(1).

https://doi.org/10.1088/2053-1591/aae3f6.

Hassan, Rakibul, M. N.I. Khan, and A. K.M.Akther Hossain. 2023. "Effect of Li Substitution on the Structural, Magnetic, and Electrical Properties of Nanocrystalline $Li_xNi_{0.6-2x}Zn_{0.4}Fe_{2+x}O_4$." J. *M. lia*

https://doi.org/10.1016/j.mtla.2023.101695.

Hossain, M. D., M. A. Hossain, and S. S. Sikder. 2022. "Hysteresis Loop Properties of Rare Earth Doped Spinel Ferrites: A Review." J. *Mag. Mag. M.* 564 (P1): 170095.

https://doi.org/10.1016/j.jmmm.2022.17005.

Hussain, Asif, Muhammad Khalid, Ali Dad Chandio, Muhammad Yasin, Nasir Abbas, M. G.B. Ashiq, Hind Albalawi, Kiran Naz, Muhammad Younas, and Beenish Masud. 2023. "Dielectrically Modified Nd^{3+} Doped (Ni–Mn) Based Spinel Ferrite $Ni_{0.5}Mn_{0.5}Nd_xFe_{2-X}O_4$ Nanoparticles for Energy Storage Applications." J. *Phys. B: Cond. Mat.* 666 (July): 415135.

https://doi.org/10.1016/j.physb.2023.41513.

Iranmanesh, P., Sh Tabatabai Yazdi, M. Mehran, and S. Saeednia. 2018. "Superior Magnetic Properties of Ni Ferrite Nanoparticles Synthesized by Capping Agent-Free One-Step Coprecipitation Route at Different PH Values." *J. Mag. Mag. M.*, 449: 172–79.

https://doi.org/10.1016/j.jmmm.2017.10.040

Kalia, S., and N. Prasad. 2023. "Overview of Properties, Applications, and Synthesis of 4d-Series Doped/Substituted Cobalt Ferrite." *Inor Chem. Comm*. 147 (November 2022): 110201.

https://doi.org/10.1016/j.inoche.2022.11021.

Kambale, R. C., K. M. Song, Y. S. Koo, and N. Hur. 2011. "Low Temperature Synthesis of Nanocrystalline Dy^{3+} Doped Cobalt Ferrite: Structural and Magnetic Properties." *J. App. Phy*., 110(5).

https://doi.org/10.1063/1.3632987.

Kokare, M. K., Nitin A. Jadhav, Yogesh Kumar, K. M. Jadhav, and S. M. Rathod. 2018. "Effect of Nd^{3+} Doping on Structural and Magnetic Properties of $Ni_{0.5}Co_{0.5}Fe_2O_4$ Nanocrystalline Ferrites Synthesized by Sol-Gel Auto Combustion Method." *J. All. Comp.* 748: 1053–61.

https://doi.org/10.1016/j.jallcom.2018.03.18.

Koutsoumbou, Xanthippi, Ioannis Tsiaoussis, Georgiana Andreea Bulai, Ovidiu Florin Caltun, Orestis Kalogirou, and Charalampos Sarafidis. 2021. "$CoFe_{2-X}RE_xO_4$ (RE=Dy, Yb, Gd) Magnetic Nanoparticles for Biomedical Applications." *J. Phys. B: Cond. Matt.* 606 (December 2020).

https://doi.org/10.1016/j.physb.2021.412849

Kumar, Lawrence, and Manoranjan Kar. 2012. "Effect of La^{3+} Substitution on the Structural and Magnetocrystalline Anisotropy of Nanocrystalline Cobalt Ferrite ($CoFe_{2-X}La_XO_4$)." Ceram Intern 38 (6): 4771–82.

https://doi.org/10.1016/j.ceramint.2012.02.065.

Kumar, Pawan, S. K. Sharma, M. Knobel, and M. Singh. 2010. "Effect of La^{3+} Doping on the Electric, Dielectric and Magnetic Properties of Cobalt Ferrite Processed by Co-Precipitation Technique." *J. All. Comp*. 508 (1): 115–18.

https://doi.org/10.1016/j.jallcom.2010.08.07.

Manohar, Ala, Krishnamoorthi Chintagumpala, and Ki Hyeon Kim. 2021. "Mixed Zn–Ni Spinel Ferrites: Structure, Magnetic Hyperthermia and Photocatalytic Properties." J. C. Int. 47 (5): 7052–61.

https://doi.org/https://doi.org/10.1016/j.ceramint.2020.11.056.

Narang, Sukhleen Bindra, and Kunal Pubby. 2021. "Nickel Spinel Ferrites: A Review." *J. Magn. Mag Mate* 519: 167163. https://doi.org/https://doi.org/10.1016/j.jmmm.2020.167163.

Óvári, Mihály, Gergely Tarsoly, Zoltán Németh, Victor G. Mihucz, and Gyula Záray. 2017. "Investigation of Lanthanum-Strontium-Cobalt Ferrites Using Laser Ablation Inductively Coupled Plasma-Mass Spectrometry." *J. Spec. B. Atom. Spec.*. 127: 42–47.

https://doi.org/10.1016/j.sab.2016.11.010.

Q. Tariq, A. S. Saleemi, M. Saeed & M. Anis-ur-Rehman. 2015. "Effect of Sintering on Co-Precipitated Nanoparticles of Mn Ferrite," 971–75.

https://doi.org/10.1007/s10948-014-2883-7.

Pubby, Kunal, K. Vijay Babu, and Sukhleen Bindra Narang. 2020. "Magnetic, Elastic, Dielectric,

Microwave Absorption and Optical Characterization of Cobalt-Substituted Nickel Spinel Ferrites." *J. M. Sci. Eng.* B: 255 (January): 114513.

https://doi.org/10.1016/j.mseb.2020.114513.

Ramadevi, P., F. Kousi, A. Sangeetha, M. Stalin Mano Gibson, and Ra Shanmugavadivu. 2019. "Structural and Electrochemical Investigation on Pure and Nickel Doped Cobalt Ferrite Nanoparticles for Supercapacitor Application." *J. M. Tod* 33: 2238–43.

https://doi.org/10.1016/j.matpr.2020.04.050.

Rana, Garima, Pooja Dhiman, Amit Kumar, Dai Viet N. Vo, Gaurav Sharma, Shweta Sharma, and Mu Naushad. 2021. "Recent Advances on Nickel Nano-Ferrite: A Review on Processing Techniques, Properties and Diverse Applications." J. *Chem. Eng. Res. Des*.175: 182–208.

https://doi.org/10.1016/j.cherd.2021.08.040.

Routray, Krutika L., Sunirmal Saha, and Dhrubananda Behera. 2020. "Nanosized $CoFe_2O_4$-Graphene Nanoplatelets with Massive Dielectric Enhancement for High Frequency Device Application." J. *M. Sci. Eng*. B 257 (April 2018): 114548.

https://doi.org/10.1016/j.mseb.2020.114548.

Sarmah, Sikha, K. P. Patra, P. K. Maji, S. Ravi, and Tribedi Bora. 2023. "A Comparative Study on the Structural, Magnetic and Dielectric Properties of Magnesium Substituted Cobalt Ferrites." *J. C. Int*. 49 (1): 1444–63.

https://doi.org/10.1016/j.ceramint.2022.09.126.

Slatineanu, Tamara, Alexandra Raluca Iordan, Victor Oancea, Mircea Nicolae Palamaru, Ioan Dumitru, Cristin Petrica Constantin, and Ovidiu Florin Caltun. 2013. "Magnetic and Dielectric Properties of Co-Zn Ferrite." J. *Mat. Sci. Eng. B* 178 (16): 1040–47.

https://doi.org/10.1016/j.mseb.2013.06.014.

Vinod, G., K. Rajashekhar, and J. Laxman Naik. 2023. "Dysprosium Doped $Cu_{0.8}Cd_{0.2}Dy_xFe_{2-X}O_4$ Nano Ferrites: A Combined Impact of Dy^{3+} on Enhanced Physical, Optical, Magnetic, and DC-Electrical Properties." *J. C. Int*. 49 (2): 2829–51.

https://doi.org/10.1016/j.ceramint.2022.09.265.

Yi, Xuwu, Minghui Cui, Yuandong Peng, Chao Xia, Zhixin Yao, and Qingbo Li. 2021. "Influence of Calcination Temperature on Microstructure and Properties of $(NiCuZn)Fe_2O_4$ Ferrite Prepared via Ultrasonic-Assisted Co-Precipitation." *J. Sup. Nov. Mag.* 34 (4): 1245–52.

https://doi.org/10.1007/s10948-021-05835-9.

Zhang, Wenhao, Jie Li, Shiwen Yi, Peng Zu, Jingxuan Wu, Jiawei Lin, Min Li, and Wenrou Su. 2021. "Influence of La-Nb Co-Substituted Sr Ferrite on Microstructure, Spectrum and Magnetic Properties of Hexaferrites." *J. All Comp*. 871: 159563.

https://doi.org/10.1016/j.jallcom.2021.159563.

التركيب، التوصيف، والخصائص الكهربية لفريتات النيكل-الكوبالت- السترونشيوم المستبدل باللانثانوم مع التطبيقات المحتملة

نيهال إبراهيم، اسيل الطراونه، د/ حاتم ابوشعيشع، ا.د/ اسامه حميده، ا.د/ حسنين اللباني، د/ماجده ذكي، د/محمد الششتاوي سالم.

تم تخليط مجموعة من عينات $Ni_{0.45}Co_{0.45}Sr_{0.1}La_xFe_{2-x}O_4$، مع قيم متغيرة للمتغير x (0.00, 0.02, 0.04, 0.06, 0.08, 0.10)، باستخدام طريقة الاحتراق التلقائي السريع. تم التحقق من وجود أيون La^{+3} المستبدل في النظام من خلال تقنيات متعددة للتوصيف، مثل المجهر الإلكتروني (SEM)، وتحليل الأشعة السينية (EDX)، وتحليل العوازل، وتحليل الخواص الكهربية. تم فحص هيئة جميع العينات باستخدام المجهر الإلكتروني بالانبعاث الحقلي (FE-SEM). زادت حجم الحبيبات المقاسة من SEM بزيادة محتوى اللانثانوم حتى x = 0.04، ثم انخفضت فوق هذه القيمة. أكدت طيفية الانتشار الطاقوي (EDX) تواجد Co Ni Sr Fe لـ x = 0.00 وأشارت إلى وجود هذه العناصر إلى جانب أيون اللانثانوم في العينات الأخرى، دون وجود اى عناصر اخرى. تم دراسة ثوابت العزل عند درجة حرارة الغرفة لجميع العينات في نطاق من 10^{-2} إلى 10^{8} هرتز. عند التردد العالي، زادت سرعة القفز وأصبح المادة الفيرايت أكثر توصيلًا، مما أدى إلى انخفاض سريع في ε' وε". عند الترددات الأقل، يؤدي إدراج كميات أعلى من اللانثانوم إلى تقليل قيم كل من ε' وε". ارتفاع محتوى اللانثانوم مرتبط بانخفاض في التوصيل الكهربائي، والذي يمكن أن يُرجع إلى القاعدة التي تحكم زيادة مقاومة الحبيبات، مما يؤدي إلى انخفاض في التوصيل المتردد. يزيد التوصيل الحراري والتموج الحراري مع ارتفاع الحرارة. نظرًا لخصائصه، يمكن أن يكون هذا المواد مثاليًا لمستشعرات ومفاتيح الحرارة والكهرومغناطيسية.